Eigenvalue repulsions in the quasinormal spectra of the Kerr-Newman black hole

Óscar J. C. Dias
STAG Research Centre and Mathematical Sciences, University of Southampton, Highfield Campus, Southampton SO17 1BJ, United Kingdom

Mahdi Godazgar
School of Mathematical Sciences, Queen Mary University of London, Mile End Road, London E1 4NS, United Kingdom

Jorge E. Santos
DAMTP, Centre for Mathematical Sciences, University of Cambridge, Wilberforce Road, Cambridge CB3 0WA, United Kingdom

Gregorio Carullo and Walter Del Pozzo
Dipartimento di Fisica "Enrico Fermi", Università di Pisa, Pisa I-56127, Italy and INFN sezione di Pisa, Pisa I-56127, Italy

Danny Laghi
Dipartimento di Fisica "Enrico Fermi", Università di Pisa, Pisa I-56127, Italy INFN sezione di Pisa, Pisa I-56127, Italy and Laboratoire des 2 Infinis - Toulouse (L2IT-IN2P3), Université de Toulouse, CNRS, UPS, F-31062 Toulouse Cedex 9, France

(Received 9 October 2021; accepted 5 April 2022; published 25 April 2022)

We study the gravito-electromagnetic perturbations of the Kerr-Newman (KN) black hole and identify the two—photon sphere and near-horizon—families of quasinormal modes (QNMs) of the black hole, computing the frequency spectra (for all the KN parameter space) of the modes with the slowest decay rate. We uncover a novel phenomenon for QNMs that is unique to the KN system, namely eigenvalue repulsion between QNM families. Such a feature is common in solid state physics where e.g., it is responsible for energy bands/gaps in the spectra of electrons moving in certain Schrödinger potentials. Exploiting the enhanced symmetries of the near-horizon limit of the near-extremal KN geometry, we also develop a matched asymptotic expansion that allows us to solve the perturbation problem using separation of variables and provides an excellent approximation to the KN QNM spectra near extremality. The KN QNM spectra derived here are needed not only to account for gravitational emission in astrophysical environments, such as the ones probed by LIGO, Virgo and LISA, but also to allow one to extract observational implications of several new physics scenarios, such as minicharged dark-matter or certain modified theories of gravity, whose observables degenerate to those of the KN solution at the scale of binary mergers.

DOI: 10.1103/PhysRevD.105.084044

I. INTRODUCTION

The black hole (BH) uniqueness theorems single out the Kerr-Newman (KN) solution as the most general regular, stationary, analytic and asymptotically flat electro-vacuum solution of Einstein-Maxwells equations [1]. Nevertheless, astrophysical BHs are not expected to be able to retain a significant amount of electric charge [2,3]. Consequently, all LIGO-Virgo [4,5] observations of events compatible with BH binaries [6] have been so far described under the assumption that the merging objects can be modeled by the Kerr metric, the zero-charge limit of the KN solution. Due to the lack of template models describing coalescing KN BHs (especially in the merger-ringdown regime), the zero-charge assumption has not yet been verified in full on observational data; although see Refs. [7,8] for recent work in this direction. Gravitational-wave (GW) observations of BH mergers are now probing the largest curvature regimes ever reached, enabling the experimental study of gravity in its strong-field and dynamical regime [6,9] and opening an observational window on potential unobserved gravitational phenomena. Here, we further the characterization of KN solutions by finding the full gravito-electromagnetic

quasinormal mode (QNM) spectra of KN BHs for the slowest decaying modes and for the full range of the KN 2-parameter space. The determination of the QNM spectrum requires solving a coupled system of two partial differential equations (PDEs) for two gauge invariant Newman-Penrose (NP) fields [10] that, upon gauge fixing, reduce to the PDE system originally found by Chandrasekhar [11,12].

Perturbative results in the small rotation parameter a [13,14] and in the small charge parameter Q [12] expansions about the Reissner-Nordström (RN) and Kerr backgrounds are available. Moreover, in [10], a numerical search of KN modes has been performed in regions of the KN parameter space that could be more prone to developing an *instability*, finding none and thus providing evidence for the linear mode stability of KN (further supported by the non-linear time evolution study of [15]). In this manuscript, we complete the search initiated in [10] and compute the frequency spectra, across the *full* KN 2-parameter space, of the most dominant (i.e., with slowest decay rates) gravito-electromagnetic QNM families (as described below, there are two main families). These are the modes that reduce—in Chandrasekhar's notation [11]—to the $Z_2, \ell = m = 2, n = 0$ modes in the Schwarzschild limit ($a = Q = 0$), where the harmonic number ℓ gives the number of zeros of the eigenfunction along the polar direction and n is the radial overtone (a and Q are the rotation and charge parameters of KN). In this process we find that, for $\ell = m = 2, n = 0$, KN has two families of QNMs. We coin these families as (1) the *photon sphere* (PS), and (2) the *near-horizon* (NH) families, although the sharp distinction between the PS and NH modes is unambiguous only for small rotation a, i.e., when the KN 2-parameter black hole is close to the Reissner-Nordström 1-parameter family.

In the Reissner-Nordström case, the PS family of QNMs is singled out because, in the eikonal or geometric optics limit (i.e., the WKB limit $m = \ell \to \infty$) it has a frequency spectrum that is closely connected to the properties of unstable equatorial circular photon orbits [16–27]. On the other hand, the NH family of QNMs distinguishes itself very clearly from the PS family because: (i) its wave-function near extremality is very much localized near the horizon and decays rapidly to zero away from the horizon, and (ii) its QNM spectrum has an imaginary part that vanishes in the extremal limit (moreover, in the Reissner-Nordström case, the NH frequency has a vanishing real part, unlike the PS modes).

It follows that to explore the PS and NH QNM families in the KN background, we start by identifying them in the Reissner-Nordström black hole. Here, the NH QNM family has the slowest decay rate very close to extremality where the charge attains its maximum value (and where the temperature vanishes) but, as we decrease the charge Q, the PS QNM family becomes the dominant solution: the two QNM curves intersect and trade dominance at a critical charge. We then switch on the rotation a and follow these two families of QNMs as each one of them spans a surface in the 2-dimensional parameter space of the KN black hole. In particular, we identify these surfaces as they run from the Reissner-Nordström limit (with $a = 0$, $Q \neq 0$) all the way to the Kerr limit (with $a \neq 0$, $Q = 0$). Interestingly, we will find that as we move toward the Kerr limit, the PS and NH families lose their individual identities. They start interacting with each other and at a certain point the two families of QNMs with the two slowest decay rates can be seen as a *combination* of what were the PS and NH modes in the Reissner-Nordström limit. Thus, this work solves a long-standing QNM puzzle. Indeed, there are hints in the literature (not made very precise) that PS and NH QNMs modes should coexist and eventually compete in the Reissner-Nordström case. It was also known that in the Kerr case there are two families of modes: the "damped modes" and "zero-damped modes" of [26,28,29]. But it had not been understood how the latter are related to the PS and NH modes of the Reissner-Nordström black hole. With our computation of the full QNM spectra, we will address this problem accurately because we will follow the families of QNMs along the full 2-parameter space of the KN black hole between its two distinguished 1-parameter limits. While doing so, we find that, remarkably, the KN frequency spectra—unlike its $a = 0$ and/or $Q = 0$ limits—are populated with intricate phenomena known as *eigenvalue repulsions*. These are ultimately responsible for the fact that the PS and NH families of Reissner-Nordström lose their individual identities and typically combine to form new 'PS-NH' QNM families as we move along the KN phase space toward the Kerr limit.

Besides computing numerically the QNM spectra for the $\ell = m = 2, n = 0$ gravito-electromagnetic QNMs, we will also use analytical methods to compute the PS and NH QNMs or the PS-NH modes in some limits. These analytical approximations match well our numerical results in the regime of parameters where they are valid and they contribute significantly to understanding the origin and distinction between the two QNMs families. For the PS case, the QNM spectrum for $\ell = m = 2$ is well approximated by the frequencies computed in the eikonal or geometric optics: the real and imaginary parts of the PS frequency are proportional to the Keplerian frequency and to the Lyapunov exponent of the orbit, respectively [26,27,30]. On the other hand, the NH QNM spectrum near extremality is well approximated by a matched asymptotic expansion that explores the enhanced symmetries of the near-horizon limit of the near-extremal KN geometry and allows us to solve the perturbation problem using separation of variables. In this manuscript, we will present the final formula for these frequencies (its derivation will be given in [30]) and compare them with the numerical data. Moreover, in [30] we will also give the QNM frequencies for other values of ℓ, m, n to have a

wider characterization of the KN QNM spectra (and this will also allows us to further discuss the eigenvalue repulsion phenomena between the different modes).

Beyond studying the fundamental properties of the slowest decaying QNMs of KN, our results are of interest for the interpretation of observational data and for applications in both ground and space-based GW detectors [4,5,31–34]. Indeed, the observational applications of our results are not limited to modeling the GW emission in realistic astrophysical environments, but include the possibility of constraining certain dark matter [35] and modified gravity [8] models. The full implications of these results to GW observations are explored in a companion paper [36].

II. FORMULATION OF THE PROBLEM

The KN BH solution can be described in standard Boyer-Lindquist coordinates $\{t, r, \theta, \phi\}$ (time, radial, polar, azimuthal coordinates) [37]. The Killing vector $K = \partial_t + \Omega_H \partial_\phi$ generates the event horizon with angular velocity Ω_H and temperature T_H. The event horizon location r_+ is the largest root of the function Δ. In terms of the mass, rotation, and charge parameters $\{M, a, Q\}$, these quantities are

$$\Delta = r^2 - 2Mr + a^2 + Q^2, \qquad r_\pm = M \pm \sqrt{M^2 - a^2 - Q^2},$$
$$\Omega_H = \frac{a}{r_+^2 + a^2}, \qquad T_H = \frac{1}{4\pi r_+}\frac{r_+^2 - a^2 - Q^2}{r_+^2 + a^2}. \tag{1}$$

At $r_- = r_+$, i.e., $a = a_{\rm ext} = \sqrt{M^2 - Q^2}$, the KN BH has a regular extremal ("ext") configuration with $T_H^{\rm ext} = 0$, and maximum angular velocity $\Omega_H^{\rm ext} = a_{\rm ext}/(M^2 + a_{\rm ext}^2)$.

Since ∂_t, ∂_ϕ are Killing vector fields of KN, its gravito-electromagnetic perturbations can be Fourier decomposed as $e^{-i\omega t}e^{im\phi}$, where ω and m are the frequency and azimuthal quantum number of the mode. Using the NP formalism, [10] derived a set of two coupled PDEs for two gauge invariant quantities ψ_{-2} and ψ_{-1} that describe the most general perturbations (except for trivial modes that shift the parameters of the solution) of a KN BH, namely:

$$(\mathcal{F}_{-2} + Q^2\mathcal{G}_{-2})\psi_{-2} + Q^2\mathcal{H}_{-2}\psi_{-1} = 0,$$
$$(\mathcal{F}_{-1} + Q^2\mathcal{G}_{-1})\psi_{-1} + Q^2\mathcal{H}_{-1}\psi_{-2} = 0, \tag{2}$$

where the second order differential operators $\{\mathcal{F}, \mathcal{G}, \mathcal{H}\}$ are in Eq. (A4) of the Appendix. The gauge invariant (under diffeomorphisms and NP tetrad rotations) perturbed quantities ψ_{-2} and ψ_{-1} are a combination of NP scalars Ψ's and Φ's (see (A2) of Appendix).

To solve the coupled PDEs (2), we need to impose physical boundary conditions. At spatial infinity, we require only outgoing waves, and at the future event horizon, we keep only regular modes in ingoing Eddington-Finkelstein coordinates. Finally, we must require regularity at the North (South) pole $\theta = \pi(-\pi)$. See Appendix for more details.

A scaling symmetry of the system allows us to work with the adimensional parameters $\{\tilde{a}, \tilde{Q}, \tilde{\omega}\} \equiv \{a/M, Q/M, \omega M\}$ (or $\{\hat{a}, \hat{Q}, \hat{\omega}\} \equiv \{a/r_+, Q/r_+, \omega r_+\}$). The $t - \phi$ symmetry of KN means that we need only consider modes with $\mathrm{Re}(\omega) \geq 0$, as long as we study both signs of m [38]. To solve the PDE problem numerically, we use a pseudospectral method that searches directly for specific QNMs using a Newton-Raphson root-finding algorithm. We refer to the review [39] and [40–42] for details. The exponential convergence of the method, and the use of quadruple precision, guarantee that the results are accurate up to, at least, the eighth decimal place.

III. ANALYTICAL ANALYSIS AND EIGENVALUE REPULSION

There are regimes of the parameter space where the frequency of the QNMs can be well approximated by analytical formulae obtained from perturbation/WKB expansions. This helps identify different families of QNMs. There are two main families of QNMs: (1) the *photon sphere* (PS), and (2) the *near-horizon* (NH) families. However, as we will find later, this sharp distinction is unambiguous only for small values of the rotation parameter. In particular, we can see this clearly for the $a = 0$ Reissner-Nordström (RN) case, the imaginary part of the frequency spectra of which is shown in the left panel of Fig. 1 (in units of r_+ since some curves change too much in a small range of charge if we use units of M) [43]. Letting $n = 0, 1, \ldots$ denote the radial overtone, the orange diamond and dark-red triangle curves describe the $n = 0$ (PS_0) and $n = 1$ (PS_1) PS families, respectively. And, the green circle and blue square curves describe the $n = 0$ (NH_0) and $n = 1$ (NH_1) NH families. Focusing our attention on the families with slowest decay rate, the PS_0 and NH_0 curves intersect (simple crossover) at $\hat{Q} = \hat{Q}_c^{\rm RN} \simeq 0.959227$ ($\tilde{Q} \equiv \tilde{Q}_c^{\rm RN} \simeq 0.9991342$). For $0 \leq \hat{Q} < \hat{Q}_c^{\rm RN}$, PS_0 is the dominant QNM, while for $\hat{Q}_c^{\rm RN} \leq \hat{Q} \leq 1$ it is the NH_0 QNM that has smaller $|\mathrm{Im}\hat{\omega}|$.

In the eikonal or geometric optics limit (the WKB limit $\ell \sim |m| \gg 1$) the PS QNM frequencies are known to be related to the properties of the equatorial plane unstable circular photon orbits. The real and imaginary parts of the PS frequency are proportional to the Keplerian frequency Ω_c and to the Lyapunov exponent λ_L, respectively [16–25]. The latter describes how quickly a null geodesic congruence around the orbit increases its cross section under radial deformations. In this limit, the PS frequencies are (see [26,27,30])

$$\omega_{\rm PS}^{\rm eikn} \simeq \frac{m}{b_s} - i\frac{n + 1/2}{b_s r_s^2}\frac{|r_s^2 + a^2 - ab_s|}{|b_s - a|(6r_s^2 + a^2 - b_s^2)^{-\frac{1}{2}}}, \tag{3}$$

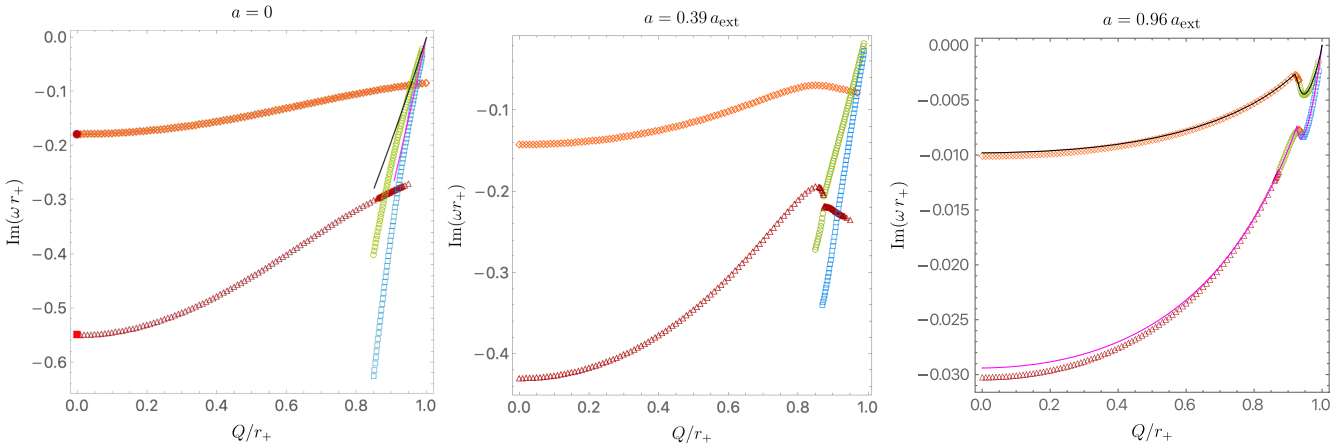

FIG. 1. QNM spectra for KN BHs with $a/a_{\rm ext} = 0$ (left), 0.39 (middle) and 0.96 (right). In the RN case, there is an unambiguous QNM family classification: the orange diamond (dark-red triangle) curve is the $n = 0$ ($n = 1$) PS family which reduces to the dark-red disk $\omega r_+ = 0.74734337 - 0.17792463i$ (red square $\omega r_+ = 0.69342199 - 0.54782975i$) in the Schwarzschild limit [11,47]. The green circle (blue square) curve is the $n = 0$ ($n = 1$) NH family (not shown: for $\hat{Q} < 0.85$ these curves extend to lower $\mathrm{Im}\hat{\omega}$). In the middle and right panels one observes eigenvalue repulsions unique to the KN QNM spectra. On the left/right panels we also show the frequency $\tilde{\omega}_{\rm NH}^{\rm MAE}$ given by (5) for $n = 0$ (black solid curve) and for $n = 1$ (magenta solid curve).

where r_s and b_s are the radius and impact parameter of the unstable orbits defined implicitly in terms of M, Q:

$$M = \frac{r_s(b_s^2 - a^2 - 2r_s^2)}{(b_s - a)^2}, \qquad Q = \frac{r_s\sqrt{b_s^2 - a^2 - 3r_s^2}}{\sqrt{(b_s - a)^2}}. \tag{4}$$

There are two real roots r_s higher than r_+ which are in correspondence with two PS modes: the *corotating* one (with $m = \ell$) that maps to the eikonal orbit with radius $r_s = r_s^-$ and $b_s > 0$ (and that has the lowest $|\mathrm{Im}\tilde{\omega}|$) and the *counterrotating* mode with $m = -\ell$ which is in correspondence with the orbit with radius $r_s = r_s^+$ and $b_s < 0$, with $r_s^+ \geq r_s^- \geq r_+$. As a check, we find that (3) is in excellent agreement with the numerical data for $\ell = m = 6$ (see [30]), and it still gives a reasonable approximation when $\ell = m = 2$. Altogether, this identifies the PS QNM family and validates our numerics.

Now let us discuss the NH family of QNMs. In the RN case (left panel of Fig. 1), this is the dominant QNM near extremality, i.e., for $\hat{Q}_c^{\rm RN} < \hat{Q} \leq 1$. Near extremality, the RN and KN near-horizon QNM wave functions are very localized near the horizon and quickly decay to zero away from it. This suggests doing a poor-man's matched asymptotic expansion (MAE), whereby we take the *near-horizon limit* of the perturbed equations (2) to find the near-region solution (which we solve analytically) and match with a *vanishing* far-region wave function in the overlapping region where both solutions are valid [48]. In fact, motivated by the result that the near-horizon limit of the extremal KN BH corresponds to a warped circle fibred over AdS_2 (anti–de Sitter) [49], the perturbations of which can be decomposed as a sum of known radial AdS_2 harmonics, we can use *separation of variables*. Therefore, the system of 2 coupled PDEs for $\{\psi_{-2}, \psi_{-1}\}$ separates into a system of 2 decoupled radial ordinary differential equations (ODEs) and a coupled system of 2 angular ODEs. This yields an analytical expression for the NH frequency (its long derivation is given in [30]):

$$\tilde{\omega}_{\rm NH}^{\rm MAE} \simeq \frac{m\tilde{a}}{1+\tilde{a}^2} + \sigma\left[\frac{m\tilde{a}(1-\tilde{a}^2)}{2(1+\tilde{a}^2)^2} - \frac{i}{4}\frac{1+2n}{1+\tilde{a}^2} - \frac{\sqrt{-\lambda_2}}{4(1+\tilde{a}^2)^2}\right] \tag{5}$$

where $n = 0, 1, 2, \ldots$ is again the radial overtone, here $\tilde{a} = \tilde{a}_{\rm ext}$, and the expansion is over the off-extremality parameter $\sigma = 1 - \frac{r_-}{r_+}$ up to $\mathcal{O}(\sigma^2)$. Here, $\lambda_2(m, \tilde{a}_{\rm ext})$ is a separation constant that we find by solving numerically the aforementioned coupled system of two angular ODEs. In our conventions, $\mathrm{Re}(\sqrt{z}) > 0$ and $\mathrm{Im}(\sqrt{z}) > 0$ when z is positive and negative, respectively. Our initial derivation of (5) is valid for $\lambda_2 > 0$ but, motivated by the Kerr results reported in [28,29,50], we will use it also when $\lambda_2 < 0$ [51]. In a complementary manner, in the WKB limit $m \gg 1$, λ_2 is well approximated by

$$\lambda_2^{\rm WKB} = \lambda_{2,0}m^2 + \lambda_{2,1}m + \lambda_{2,2} + \frac{\lambda_{2,3}}{m} + \mathcal{O}(1/m^2), \tag{6}$$

where the WKB coefficients $\lambda_{2,0}, \ldots, \lambda_{2,4}$ are functions of $\tilde{a}$ given in (A6) of the Appendix. At extremality ($\sigma = 0$), (5) reduces to $\mathrm{Re}\tilde{\omega} = m\tilde{\Omega}_H^{\rm ext}$ and $\mathrm{Im}\tilde{\omega} = 0$, and in the Kerr and RN limits, it reduces to the expressions first found in [26,28,29], respectively.

Approximation (5) is in excellent agreement with the numerical frequencies (near extremality). This is illustrated in the left and right panels of Fig. 1. For the RN case

(left panel), extremality is at $\hat{Q}=1$ and (5) with $n=0$ (black line) gives the correct slope for the NH_0 family (green circles), while (5) with $n=1$ (magenta line) yields the slope of the NH_1 family (blue squares). On the right panel, we take a KN BH family with $a/a_{\rm ext}=0.96$ (so the whole family of solutions is close to extremality) and compare the numerical results for the dominant $n=0$ QNMs (curve that connects orange diamonds and green circles) with the black curve, i.e., (5) with $n=0$. Moreover, we also compare (5) with $n=1$ (magenta curve) with the $n=1$ numerical modes with the second slowest decay rate (3-branched curve connecting the dark-red triangles, green circles and blue squares). So, (5) clearly identifies the NH family in the RN limit, and more generically, the dominant modes near extremality.

Figure 1 illustrates a remarkable property of KN QNMs. In the RN case (left panel) and for small rotation, the PS_0 family dominates the spectra for $0\leq\tilde{Q}<\tilde{Q}_c(\tilde{a})$ (with $\tilde{Q}_c(0)=\tilde{Q}_c^{\rm RN}$) while the NH_0 family dominates for $\tilde{Q}_c(\tilde{a})<\tilde{Q}\leq 1$. But, when $\tilde{a}$ grows and approaches to extremality, e.g., at $a/a_{\rm ext}=0.96$ (right panel), the PS_0 family *merges* with the NH_0 family (i.e., orange diamond and green circle curves merge in the right panel of Fig. 1). For higher $a/a_{\rm ext}$ the two families remain merged and this line of solutions approaches $\mathrm{Im}\tilde{\omega}=0$, $\mathrm{Re}\tilde{\omega}=m\tilde{\Omega}_H^{\rm ext}$ as $a\to a_{\rm ext}$. The whole $n=0$ QNM curve in the right plot is thus well approximated by (5): it captures the NH_0 modes in the RN limit but also the "PS_0-NH_0 merged" modes (when close to extremality).

The above features of the KN QNMs can be best understood in terms of a critical rotation $\tilde{a}_\star$ (or critical charge $\tilde{Q}_\star=\sqrt{1-\tilde{a}_\star^2}$) in relation to the extremal rotation $\tilde{a}_{\rm ext}$ (or extremal charge $\tilde{Q}_{\rm ext}$). When $\tilde{a}_\star<\tilde{a}_{\rm ext}\leq 1$ ($0\leq\tilde{Q}_{\rm ext}<\tilde{Q}_\star$), as is the case in the Kerr limit where $\tilde{a}_{\rm ext}=1$, the PS family terminates at $\mathrm{Im}\tilde{\omega}=0$ and $\mathrm{Re}\tilde{\omega}=m\tilde{\Omega}_H^{\rm ext}$ at extremality. However, when $\tilde{a}_\star>\tilde{a}_{\rm ext}$ ($\tilde{Q}_\star<\tilde{Q}_{\rm ext}$), as is the case in the RN limit where $\tilde{Q}_{\rm ext}=1$, the PS family falls short of the $(\mathrm{Im}\tilde{\omega},\mathrm{Re}\tilde{\omega})=(0,m\tilde{\Omega}_H^{\rm ext})$ surface at extremality.

Interestingly, the $\star$ transition point turns out to be given (within numerical error) by the point where the separation constant $\lambda_2(m,\tilde{a}_{\rm ext})$ in (5) vanishes: $\lambda_2(m,\tilde{a}_\star^{\rm NH})=0$ ($\lambda_2>0$ for $\tilde{a}_{\rm ext}<\tilde{a}_\star^{\rm NH}$; $\lambda_2<0$ for $\tilde{a}_{\rm ext}>\tilde{a}_\star^{\rm NH}$). To get accurate values for $\tilde{a}_\star^{\rm NH}$ we use the numerical solution for λ_2. Alternatively, we get a good approximation by using the WKB result (6) for λ_2:

$$\tilde{a}_\star^{\rm NH}|_{\rm WKB}\sim\frac{1}{2}-\frac{5\sqrt{3}(2-\sqrt{2})}{32m}+\frac{5(69-176\sqrt{2})}{2048m^2}+\mathcal{O}(m^{-3}) \tag{7}$$

In the first case we get $\{\tilde{a}_\star,\tilde{Q}_\star\}^{\rm NH}\simeq\{0.360,0.932\}$ while (7) yields $\{\tilde{a}_\star,\tilde{Q}_\star\}^{\rm NH}_{\rm WKB}\sim\{0.311,0.970\}$ (for $m=2$) [54].

In summary, our analysis uncovers a surprising property not observed in the QNM spectra of Schwarzschild, Kerr or RN. Indeed, in the KN QNM spectra we observe a phenomenon know as *eigenvalue repulsion* [55]. The latter is common in solid state physics when e.g., electrons move in certain Schrödinger potentials that introduce energy bands/gaps (see e.g., Sec. 7 of [58]). The eigenvalue repulsion feature is most evident by considering the evolution of the 3 plots in Fig. 1. In the RN case (left plot), and for small rotation, we have a sharp and unambiguous distinction between the four families of modes represented. In particular, the PS_0 family dominates the spectra for $0\leq\hat{Q}<\hat{Q}_c(\hat{a})$ (with $\hat{Q}_c(0)=\hat{Q}_c^{\rm RN}$) while the NH_0 family dominates for $\hat{Q}_c(\hat{a})<\hat{Q}\leq 1$. The two modes intersect at $\hat{Q}=\hat{Q}_c(\hat{a})$ with a simple crossover and similar crossovers occur when the PS_1 curve intersects the NH_0 or NH_1 curves. However, at $a/a_{\rm ext}=0.39$ (middle panel), we find that eigenvalue repulsion occurs between the PS_1 and NH_0 families: the PS_1 curve breaks into two pieces and the same occurs for the NH_0 curve. The left (right) branch of the PS_1 family now connects to the right (left) branch of the NH_0 curve and a *frequency gap* appears between the two new curves in the neighborhood of the two associated kinks. The distinction between the families is no longer sharp. As the rotation increases, new eigenvalue repulsions occur. For example, at $a/a_{\rm ext}=0.96$, the PS_0 curve breaks into two pieces and the same occurs (again) for the NH_0 curve. The left branch of the PS_0 family now merges with the right branch of the NH_0 curve and this new curve is well described by the black curve (5) (not shown: the right branch of the PS_0 curve merges with a $n>1$ NH curve). Below, the left branch of the NH_0 curve now bridges the dark-red triangle PS_1 curve with the blue square NH_1 curve (the NH_1 curve also breaks and merges with another $n>1$ curve but we do not show these further subdominant modes).

IV. FULL QNM SPECTRA

The full spectra of the most dominant KN QNMs—classified as Z_2, $\ell=m=2$, $n=0$ by [11] (Table V, page 262) in the Schwarzschild limit—is given in Fig. 2. The left/right panel gives the imaginary/real part of the frequency. The brown curve has $\mathrm{Im}\tilde{\omega}=0$, $\mathrm{Re}\tilde{\omega}=m\tilde{\Omega}_H^{\rm ext}$. To scan the 2-dimensional parameter space we used a grid with 100×100 points in $[0,1]\times[0,1]$ for $\{\hat{Q},a/a_{\rm ext}\}$ with $\hat{a}_{\rm ext}=\sqrt{1-\hat{Q}^2}$.

The KN modes with slowest decay rate always terminate at extremality along the extremal brown curve, with the frequencies off-extremality well approximated by (5) as illustrated in Fig. 1. The red surface family, continuously connected to the Schwarzschild mode (dark-red point [11,47]), is the PS_0 QNM family as we unambiguously identify it in the RN limit. It dominates the spectra for most of the parameter space. However, for large $\tilde{Q}$ it is instead

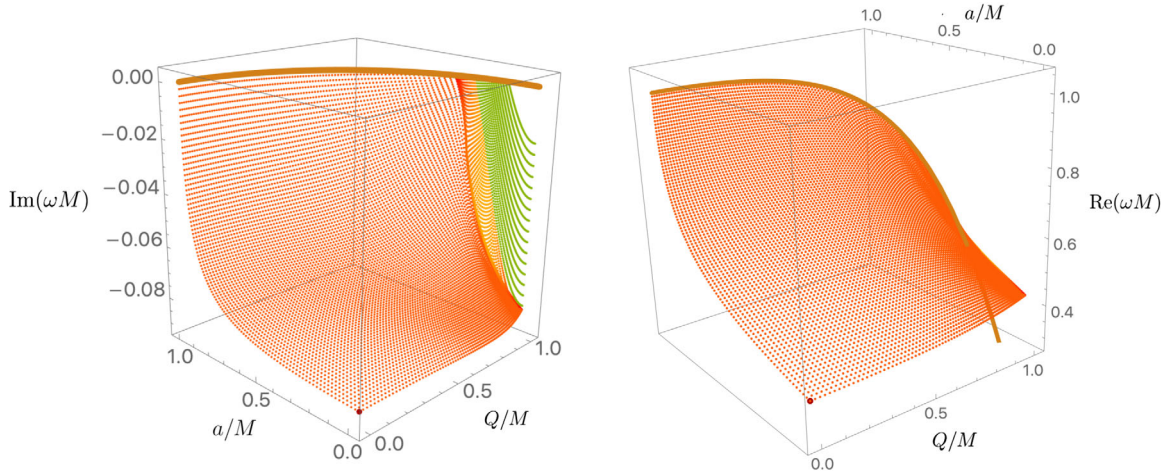

FIG. 2. Imaginary (left panel) and real (right panel) parts of the frequency for the Z_2, $\ell = m = 2$, $n = 0$ KN QNM with lowest $|\mathrm{Im}\tilde{\omega}|$. At extremality, the dominant mode always starts at $\mathrm{Im}\tilde{\omega} = 0$ and $\mathrm{Re}\tilde{\omega} = m\tilde{\Omega}_H^{\mathrm{ext}}$ (brown curve). The dark-red point ($a = 0 = Q$), $\tilde{\omega} \simeq 0.37367168 - 0.08896232i$, is the gravitational QNM of Schwarzschild [11,47]. In the right panel, the orange and green regions are so close to the extremal brown curve that they are not visible.

the NH_0 QNM family (green surface) that has the lowest $|\mathrm{Im}\tilde{\omega}|$. In between these orange/green regions there is a yellowish zone. This is where either simple crossovers (that trade mode dominance) or eigenvalue repulsions between the PS_0 and NH_0 modes occurs. These were already analysed in the discussion of Fig. 1.

Besides characterizing the fundamental properties of linear perturbations of the KN black hole, the derived QNM spectra can be used to model beyond Standard Model physics in binary mergers and GW emission in realistic astrophysical environments, bearing increasing importance with future enhancements in sensitivity of current and planned GW observatories. In a companion paper [36], we apply the results obtained in this work to the latest observations from the GW detector network.

ACKNOWLEDGMENTS

The authors would like to thank Nathan Johnson-McDaniel for helpful discussions. We acknowledge the use of the cluster "Baltasar-Sete-Sóis," and associated support services at CENTRA/IST, in the completion of this work. The authors further acknowledge the use of the IRIDIS High Performance Computing Facility, and associated support services at the University of Southampton, in the completion of this work. O. C. D. acknowledges financial support from the STFC "Particle Physics Grants Panel (PPGP) 2016" Grant No. ST/P000711/1 and the STFC "Particle Physics Grants Panel (PPGP) 2018" Grant No. ST/T000775/1. M. G is supported by a Royal Society University Research Fellowship. J. E. S. has been partially supported by STFC consolidated Grants No. ST/P000681/1, No. ST/T000694/1. The research leading to these results has received funding from the European Research Council under the European Community's Seventh Framework Programme (FP7/2007-2013) / ERC Grant agreement no. [247252].

APPENDIX: PDE AND WKB COEFFICIENTS

1. Coupled pair of PDEs for the KN perturbations

The uniqueness theorems [59,60] state that the Kerr-Newman (KN) black hole (BH) is the unique, most general family of stationary asymptotically flat BHs, of Einstein-Maxwell theory. It is characterized by 3 parameters: mass M, angular momentum $J \equiv Ma$ and charge Q. The Kerr, Reissner-Nordström (RN) and Schwarzschild (Schw) BHs constitute limiting cases: $Q = 0$, $a = 0$ and $Q = a = 0$, respectively. The gravitational and Maxwell fields of the KN BH in Boyer-Lindquist coordinates are given by [37,61]

$$\begin{aligned} ds^2 &= -\frac{\Delta}{\Sigma}(\mathrm{d}t - a\sin^2\theta \mathrm{d}\phi)^2 + \frac{\Sigma}{\Delta}\mathrm{d}r^2 + \Sigma \mathrm{d}\theta^2 \\ &\quad + \frac{\sin^2\theta}{\Sigma}[(r^2 + a^2)\mathrm{d}\phi - a\mathrm{d}t]^2, \\ A &= \frac{Qr}{\Sigma}(\mathrm{d}t - a\sin^2\theta \mathrm{d}\phi), \end{aligned} \tag{A1}$$

with $\Delta = r^2 - 2Mr + a^2 + Q^2$ and $\Sigma = r^2 + a^2\cos^2\theta$.

Linear gravito-electromagnetic perturbations about the KN background are more easily addressed in the Newman-Penrose (NP) formalism [62]. In the context of this formalism there is a well-known set of NP scalars built of contractions of the NP tetrad with the Weyl tensor (e.g., Ψ_2, Ψ_3 and Ψ_4) or with the Maxwell field strength (e.g., Φ_1 and Φ_2) [11,63]. Out of these, one can construct two *gauge invariant* perturbed quantities, i.e., quantities that are invariant under both linear diffeomorphisms and tetrad rotations, namely [10]:

$$\psi_{-2} = (\bar{r}^*)^4 \Psi_4^{(1)},$$
$$\psi_{-1} = \frac{(\bar{r}^*)^3}{2\sqrt{2}\Phi_1^{(0)}}(2\Phi_1^{(0)}\Psi_3^{(1)} - 3\Psi_2^{(0)}\Phi_2^{(1)}), \quad \text{(A2)}$$

with $\bar{r} = r + ia\cos\theta$. Here, NP scalars with superscript $^{(0)}$ refer to scalars in the KN background and the superscript $^{(1)}$ to first order perturbations of the scalar. These NP scalars (A2) are the ones relevant for the study of perturbations that are outgoing at future null infinity and regular at the future horizon [64]. Reference [10] derived a set of two coupled partial differential equations (PDEs) for ψ_{-2} and ψ_{-1} that describe the most general perturbations (except for trivial modes that shift the parameters of the solution) of a KN BH, namely:

$$(\mathcal{F}_{-2} + Q^2\mathcal{G}_{-2})\psi_{-2} + Q^2\mathcal{H}_{-2}\psi_{-1} = 0,$$
$$(\mathcal{F}_{-1} + Q^2\mathcal{G}_{-1})\psi_{-1} + Q^2\mathcal{H}_{-1}\psi_{-2} = 0, \quad \text{(A3)}$$

where the second order differential operators $\{\mathcal{F}, \mathcal{G}, \mathcal{H}\}$ are given by [10]

$$\begin{aligned}
\mathcal{F}_{-2} &= \Delta\mathcal{D}_{-1}^\dagger\mathcal{D}_0 + \mathcal{L}_{-1}\mathcal{L}_2^\dagger - 6i\omega\bar{r},\\
\mathcal{G}_{-2} &= \Delta\mathcal{D}_{-1}^\dagger\alpha_-\bar{r}^*\mathcal{D}_0 - 3\Delta\mathcal{D}_{-1}^\dagger\alpha_- - \mathcal{L}_{-1}\alpha_+\bar{r}^*\mathcal{L}_2^\dagger\\
&\quad + 3\mathcal{L}_{-1}\alpha_+ ia\sin\theta,\\
\mathcal{H}_{-2} &= -\Delta\mathcal{D}_{-1}^\dagger\alpha_-\bar{r}^*\mathcal{L}_{-1} - 3\Delta\mathcal{D}_{-1}^\dagger\alpha_- ia\sin\theta\\
&\quad - \mathcal{L}_{-1}\alpha_+\bar{r}^*\Delta\mathcal{D}_{-1}^\dagger - 3\mathcal{L}_{-1}\alpha_+\Delta,\\
\mathcal{F}_{-1} &= \Delta\mathcal{D}_1\mathcal{D}_{-1}^\dagger + \mathcal{L}_2^\dagger\mathcal{L}_{-1} - 6i\omega\bar{r},\\
\mathcal{G}_{-1} &= -\mathcal{D}_0\alpha_+\bar{r}^*\Delta\mathcal{D}_{-1}^\dagger - 3\mathcal{D}_0\alpha_+\Delta + \mathcal{L}_2^\dagger\alpha_-\bar{r}^*\mathcal{L}_{-1}\\
&\quad + 3\mathcal{L}_2^\dagger\alpha_- ia\sin\theta,\\
\mathcal{H}_{-1} &= -\mathcal{D}_0\alpha_+\bar{r}^*\mathcal{L}_2^\dagger + 3\mathcal{D}_0\alpha_+ ia\sin\theta\\
&\quad - \mathcal{L}_2^\dagger\alpha_-\bar{r}^*\mathcal{D}_0 + 3\mathcal{L}_2^\dagger\alpha_-, \quad \text{(A4)}
\end{aligned}$$

with $\alpha_\pm \equiv [3(\bar{r}^2M - \bar{r}Q^2) \pm Q^2\bar{r}^*]^{-1}$, and we introduced the radial and angular Chandrasekhar operators [11],

$$\mathcal{D}_j = \partial_r + \frac{iK_r}{\Delta} + 2j\frac{(r-M)}{\Delta}, \qquad K_r = am - (r^2+a^2)\omega;$$
$$\mathcal{L}_j = \partial_\theta + K_\theta + j\cot\theta, \qquad K_\theta = \frac{m}{\sin\theta} - a\omega\sin\theta. \quad \text{(A5)}$$

The complex conjugate of these operators, namely $\mathcal{D}_j^\dagger$ and $\mathcal{L}_j^\dagger$, can be obtained from $\mathcal{D}_j$ and $\mathcal{L}_j$ via the replacement $K_r \to -K_r$ and $K_\theta \to -K_\theta$, respectively.

Note that fixing a gauge in which $\Phi_0^{(1)} = \Phi_1^{(1)} = 0$, (A3) reduces to the Chandrasekhar coupled PDE system [11] (see also the derivation in [12]). Finally, note that in the limit $Q \to 0$ (A3) decouple yielding the familiar Teukolsky equation for Kerr [66].

Since $\partial_t, \partial_\phi$ are Killing vector fields of KN, we can Fourier decompose the perturbations $\{\psi_{-2}, \psi_{-1}\}$ as $e^{-i\omega t}e^{im\phi}$. This introduces the frequency ω and azimuthal quantum number m of the perturbation. The $t-\phi$ symmetry of the KN BH allows us to consider only modes with $\mathrm{Re}(\omega) \geq 0$, as long as we study both signs of m. Then, to solve the coupled PDEs (A2), we need to impose physical boundary conditions (BCs). At spatial infinity, a Frobenius analysis of (A3) that allows only outgoing waves yields the decay:

$$\psi_s|_\infty \simeq e^{i\omega r}r^{-(2s+1)+i\omega\frac{r_+^2+a^2+Q^2}{r_+}}\left(\alpha_s(\theta) + \frac{\beta_s(\theta)}{r} + \cdots\right),$$

where $s = -2, -1$, and $\beta_s(\theta)$ is a function of $\alpha_s(\theta)$ and its derivative fixed by expanding (A3) at spatial infinity.

At the horizon, a Frobenius analysis whereby we require only regular modes in ingoing Eddington-Finkelstein coordinates, yields the expansion

$$\psi_s|_H \simeq (r-r_+)^{-s-\frac{i(\omega-m\Omega_H)}{4\pi T_H}}[a_s(\theta) + b_s(\theta)(r-r_+) + \cdots],$$

where $b_s(\theta)$ is a function of $a_s(\theta)$ and its derivative.

At the North (South) pole $x \equiv \cos\theta = 1(-1)$, regularity dictates that the fields must behave as ($\varepsilon = 1$ for $|m| \geq 2$, while $\varepsilon = -1$ for $|m| = 0, 1$ modes)

$$\psi_s|_{\mathrm{N,(S)}} \simeq (1 \mp x)^{\varepsilon\frac{1\pm1}{2}\frac{s+|m|}{2}}[A_s^\pm(r) + B_s^\pm(r)(1 \mp x) + \cdots],$$

where $B_s^+(r)(B_s^-(r))$ is a function of $A_s^+(r)(A_s^-(r))$ and its derivatives along r, whose exact form is fixed by expanding (A3) around the North (South) pole.

2. WKB coefficients for the separation constant λ_2

At extremality, the modes with slowest decay rate (independently of belonging to the NH or PS families) always approach $\mathrm{Im}\tilde{\omega} = 0$ and $\mathrm{Re}\tilde{\omega} = m\tilde{\Omega}_H^{\mathrm{ext}}$ and (5) of the main text provides an excellent approximation to their frequency in an expansion off-extremality (as analyzed in the discussion of Fig. 1 of the main text). The derivation of the analytical approximation (5) of the main text is quite long and thus we will present it in the companion manuscript [30].

In (5) of the main text, the separation constant λ_2 has a WKB expansion for large m, as given in Eq. (6) of the main text. The associated WKB coefficients are

$$\lambda_{2,0} = 4(1-4\hat{a}^2), \qquad \lambda_{2,1} = -4(1+\hat{a}^2)(2\sqrt{1-\hat{a}^2} - \sqrt{1+2\hat{a}^2}), \tag{A6a}$$

$$\lambda_{2,2} = \frac{3\sqrt{1-\hat{a}^2}(1+\hat{a}^2)^2(3-726\hat{a}^{10}-253\hat{a}^8+128\hat{a}^6-74\hat{a}^4-50\hat{a}^2)}{(1+2\hat{a}^2)[(66\hat{a}^6-5\hat{a}^4-12\hat{a}^2+5)\sqrt{1-\hat{a}^2}+4(1-\hat{a}^4)\sqrt{2\hat{a}^2+1}]}, \tag{A6b}$$

$$\begin{aligned}
\lambda_{2,3} = {} & [4(1+2\hat{a}^2)^{7/2}(578577650112\hat{a}^{40} - 338129795520\hat{a}^{38} - 1042453021104\hat{a}^{36} + 1170932108544\hat{a}^{34} \\
& + 243872180244\hat{a}^{32} - 1092788709804\hat{a}^{30} + 457571937931\hat{a}^{28} + 286639850738\hat{a}^{26} - 371225227587\hat{a}^{24} \\
& + 75821376048\hat{a}^{22} + 83823143199\hat{a}^{20} - 64522516578\hat{a}^{18} + 5397537793\hat{a}^{16} + 11870759300\hat{a}^{14} - 5939331087\hat{a}^{12} \\
& + 15670254\hat{a}^{10} + 798959271\hat{a}^8 - 269248008\hat{a}^6 - 8868395\hat{a}^4 + 20327618\hat{a}^2 - 4782969) \\
& + 4\sqrt{1-\hat{a}^2}(1+2\hat{a}^2)^3(661231600128\hat{a}^{40} - 788969522880\hat{a}^{38} - 475886378880\hat{a}^{36} + 1029138506352\hat{a}^{34} \\
& - 630648141552\hat{a}^{32} - 452699156052\hat{a}^{30} + 658166339168\hat{a}^{28} - 186975958943\hat{a}^{26} - 249892000005\hat{a}^{24} \\
& + 178743692406\hat{a}^{22} - 3249242106\hat{a}^{20} - 56479482309\hat{a}^{18} + 20902690721\hat{a}^{16} + 3663601312\hat{a}^{14} - 5845481340\hat{a}^{12} \\
& + 1100552199\hat{a}^{10} + 410656173\hat{a}^8 - 279409506\hat{a}^6 + 19829366\hat{a}^4 + 13153165\hat{a}^2 - 4782969)]^{-1} \\
& \times [3\hat{a}^2\sqrt{1-\hat{a}^2}(1+\hat{a}^2)^3\sqrt{2\hat{a}^2+1}(90588729217536\hat{a}^{46} + 93586813404480\hat{a}^{44} - 64234642488192\hat{a}^{42} \\
& - 54181551934224\hat{a}^{40} + 14733709326864\hat{a}^{38} - 3470814109976\hat{a}^{36} - 897909422067\hat{a}^{34} + 34432474064505\hat{a}^{32} \\
& - 10922161747605\hat{a}^{30} - 23041644949212\hat{a}^{28} + 5136927583340\hat{a}^{26} + 4733507876355\hat{a}^{24} - 3578226571619\hat{a}^{22} \\
& - 898929274206\hat{a}^{20} + 753565243446\hat{a}^{18} - 135077374365\hat{a}^{16} - 174223122235\hat{a}^{14} + 33089919120\hat{a}^{12} \\
& + 8380363168\hat{a}^{10} - 9890782275\hat{a}^8 - 803782461\hat{a}^6 + 541670718\hat{a}^4 - 148272034\hat{a}^2 - 57395628) \\
& + 3\hat{a}^2(1+\hat{a}^2)^3(158530276130688\hat{a}^{48} + 192260601732672\hat{a}^{46} - 226279077675552\hat{a}^{44} \\
& - 257580189150768\hat{a}^{42} + 238634465705064\hat{a}^{40} + 187478664334236\hat{a}^{38} - 167948153974214\hat{a}^{36} \\
& - 79050787933609\hat{a}^{34} + 69165996968940\hat{a}^{32} + 1562277529575\hat{a}^{30} - 26149776558142\hat{a}^{28} \\
& + 6310859786413\hat{a}^{26} + 3820171951948\hat{a}^{24} - 4424582883901\hat{a}^{22} - 417658252182\hat{a}^{20} + 868831525263\hat{a}^{18} \\
& - 249677209480\hat{a}^{16} - 170706582299\hat{a}^{14} + 47404470046\hat{a}^{12} + 4708012127\hat{a}^{10} - 10932078636\hat{a}^8 - 398469675\hat{a}^6 \\
& + 532105820\hat{a}^4 - 176969858\hat{a}^2 - 57395628)].
\end{aligned} \tag{A6c}$$

The derivation of (6) of the main text and of (A6) is again long and will be given it in the companion manuscript [30]. There, we also show that this WKB expansion provides an excellent approximation already for $m = 10$ and a good approximation even for $m = 2$.

[1] P. O. Mazur, arXiv:hep-th/0101012.
[2] G. W. Gibbons, Commun. Math. Phys. **44**, 245 (1975).
[3] R. D. Blandford and R. L. Znajek, Mon. Not. R. Astron. Soc. **179**, 433 (1977).
[4] J. Aasi *et al.* (LIGO Scientific Collaboration), Classical Quantum Gravity **32**, 074001 (2015).
[5] F. Acernese *et al.* (Virgo Collaboration), Classical Quantum Gravity **32**, 024001 (2015).
[6] R. Abbott *et al.* (LIGO Scientific, Virgo Collaborations), Phys. Rev. X **11**, 021053 (2021).
[7] P. K. Gupta, T. F. M. Spieksma, P. T. H. Pang, G. Koekoek, and C. V. D. Broeck, Phys. Rev. D **104**, 063041 (2021).
[8] G. Bozzola and V. Paschalidis, Phys. Rev. Lett. **126**, 041103 (2021).
[9] R. Abbott *et al.* (LIGO Scientific, Virgo Collaborations), Phys. Rev. D **103**, 122002 (2021).
[10] O. J. C. Dias, M. Godazgar, and J. E. Santos, Phys. Rev. Lett. **114**, 151101 (2015).
[11] S. Chandrasekhar, *The Mathematical Theory of Black Holes* (Oxford Press, New York, 1983).
[12] Z. Mark, H. Yang, A. Zimmerman, and Y. Chen, Phys. Rev. D **91**, 044025 (2015).
[13] P. Pani, E. Berti, and L. Gualtieri, Phys. Rev. Lett. **110**, 241103 (2013).

[14] P. Pani, E. Berti, and L. Gualtieri, Phys. Rev. D **88**, 064048 (2013).
[15] M. Zilhão, V. Cardoso, C. Herdeiro, L. Lehner, and U. Sperhake, Phys. Rev. D **90**, 124088 (2014).
[16] C. J. Goebel, Astrophys. J. **172**, L95 (1972).
[17] V. Ferrari and B. Mashhoon, Phys. Rev. D **30**, 295 (1984).
[18] V. Ferrari and B. Mashhoon, Phys. Rev. Lett. **52**, 1361 (1984).
[19] B. Mashhoon, Phys. Rev. D **31**, 290 (1985).
[20] L. Bombelli and E. Calzetta, Classical Quantum Gravity **9**, 2573 (1992).
[21] N. J. Cornish and J. J. Levin, Classical Quantum Gravity **20**, 1649 (2003).
[22] V. Cardoso, A. S. Miranda, E. Berti, H. Witek, and V. T. Zanchin, Phys. Rev. D **79**, 064016 (2009).
[23] S. R. Dolan, Phys. Rev. D **82**, 104003 (2010).
[24] H. Yang, D. A. Nichols, F. Zhang, A. Zimmerman, Z. Zhang, and Y. Chen, Phys. Rev. D **86**, 104006 (2012).
[25] Z. Stuchlik and M. Calvani, Gen. Relativ. Gravit. **23**, 507 (1991).
[26] A. Zimmerman and Z. Mark, Phys. Rev. D **93**, 044033 (2016); **93**, 089905(E) (2016).
[27] P.-C. Li, T.-C. Lee, M. Guo, and B. Chen, Phys. Rev. D **104**, 084044 (2021).
[28] H. Yang, F. Zhang, A. Zimmerman, D. A. Nichols, E. Berti, and Y. Chen, Phys. Rev. D **87**, 041502 (2013).
[29] H. Yang, A. Zimmerman, A. Zenginolu, F. Zhang, E. Berti, and Y. Chen, Phys. Rev. D **88**, 044047 (2013).
[30] O. J. C. Dias, M. Godazgar, and J. E. Santos, Eigenvalue repulsions and quasinormal mode spectra of Kerr-Newman: An extended study (2022) (to be published).
[31] T. Akutsu *et al.* (KAGRA Collaboration), Prog. Theor. Exp. Phys. **2021**, 05A101 (2021).
[32] M. Punturo, M. Abernathy, F. Acernese, B. Allen, N. Andersson, K. Arun, F. Barone, B. Barr, M. Barsuglia, M. Beker *et al.*, Classical Quantum Gravity **27**, 194002 (2010).
[33] D. Reitze *et al.*, Bull. Am. Astron. Soc. **51**, 035 (2019).
[34] P. Amaro-Seoane, H. Audley, S. Babak, J. Baker, E. Barausse, P. Bender, E. Berti, P. Binetruy, M. Born, D. Bortoluzzi *et al.*, arXiv:1702.00786.
[35] V. Cardoso, C. F. B. Macedo, P. Pani, and V. Ferrari, J. Cosmol. Astropart. Phys. 05 (**2016**) 054.
[36] G. Carullo, D. Laghi, N. K. Johnson-McDaniel, W. Del Pozzo, O. J. C. Dias, M. Godazgar, and J. E. Santos, Phys. Rev. D **105**, 062009 (2022).
[37] T. Adamo and E. Newman, Scholarpedia **9**, 31791 (2014).
[38] When $a = 0$ this enhances to a $t \to -t$ symmetry and the QNM frequencies form pairs of $\{\omega, -\omega^*\}$.
[39] O. J. C. Dias, J. E. Santos, and B. Way, Classical Quantum Gravity **33**, 133001 (2016).
[40] O. J. Dias, P. Figueras, R. Monteiro, and J. E. Santos, Phys. Rev. D **82**, 104025 (2010).
[41] O. J. Dias, R. Monteiro, and J. E. Santos, J. High Energy Phys. 08 (2011) 139.
[42] O. J. C. Dias, G. S. Hartnett, and J. E. Santos, Classical Quantum Gravity **31**, 245011 (2014).
[43] The frequency spectra in the left panel of Fig. 1 was obtained solving the coupled pair of KN PDEs and, independently, the Regge-Wheeler-Zerilli ODE [44,45] that describes perturbations of RN. The fact that both match validates our numerics for the KN PDEs. See [46] for a detailed review on QNM studies of the RN and Kerr black holes.
[44] T. Regge and J. A. Wheeler, Phys. Rev. **108**, 1063 (1957).
[45] F. Zerilli, Phys. Rev. D **9**, 860 (1974).
[46] E. Berti, V. Cardoso, and A. O. Starinets, Classical Quantum Gravity **26**, 163001 (2009).
[47] E. Leaver, Proc. R. Soc. A **402**, 285 (1985).
[48] Ideally, we would also solve the far-region equations to obtain the subleading far-region solution but in the KN background we cannot do it analytically.
[49] J. M. Bardeen and G. T. Horowitz, Phys. Rev. D **60**, 104030 (1999).
[50] S. Hod, Phys. Rev. D **78**, 084035 (2008).
[51] The functional dependence on temperature of the near horizon QNMs has appeared in the phenomenological model of [52,53].
[52] S. Hod, Eur. Phys. J. C **75**, 272 (2015).
[53] S. Hod, Eur. Phys. J. C **75**, 611 (2015).
[54] The eikonal analysis (3) also predicts the $\star$ transition point. Namely, in the $m \to \infty$ limit it predicts $\tilde{a}_\star^{\rm eikn} = 1/2$ which is, as expected, not a good approximation to $\tilde{a}_\star \simeq 0.360$. However, in [30] we show that the curve $\tilde{a}_\star(m)$ increasingly agrees with the eikonal PS prediction (3) when m grows.
[55] It could well be that eigenvalue repulsion is also ultimately responsible for the special features displayed by (1) the $n = 5$ (i.e., $n = 6$ if we start counting them at $n = 1$) overtone of the $\ell = m = 2$ photon sphere QNM of Kerr (see Fig. 4 of [46,56]), and (2) by the QNM spectra of de Sitter RN black holes [57].
[56] H. Onozawa, Phys. Rev. D **55**, 3593 (1997).
[57] O. J. C. Dias and J. E. Santos, Phys. Rev. D **102**, 124039 (2020).
[58] C. Kittel, *Introduction to Solid State Physics*, 8th ed. (John Wiley & Sons, New York, 2004).
[59] D. Robinson, in *The Kerr Spacetime: Rotating Black Holes in General Relativity*, edited by D. L. Wiltshire, M. Visser, and S. M. Scott (Cambridge University Press, Cambridge, England, 2009).
[60] P. T. Chrusciel, J. L. Costa, and M. Heusler, Living Rev. Relativity **15**, 7 (2012).
[61] E. T. Newman, R. Couch, K. Chinnapared, A. Exton, A. Prakash, and R. Torrence, J. Math. Phys. (N.Y.) **6**, 918 (1965).
[62] E. Newman and R. Penrose, J. Math. Phys. (N.Y.) **3**, 566 (1962).
[63] H. Stephani, D. Kramer, M. A. MacCallum, C. Hoenselaers, and E. Herlt, *Exact Solutions of Einstein's Field Equations* (Cambridge University Press, Cambridge, England, 2003).
[64] There is a set of two coupled PDEs—related to (4) by a Geroch-Held-Penrose [65] transformation—for the quantities ψ_2 and ψ_1 that are the positive spin counterparts of (4); however these would be relevant if we were interested in perturbations that were outgoing at past null infinity.
[65] R. P. Geroch, A. Held, and R. Penrose, J. Math. Phys. (N.Y.) **14**, 874 (1973).
[66] S. Teukolsky, Phys. Rev. Lett. **29**, 1114 (1972).